Influence of ammonia oxidation rate on thaumarchaeal lipid composition and the TEX_{86} temperature proxy

Sarah J. Hurley[a,1,2], Felix J. Elling[b,c,1,2], Martin Könneke[b,c], Carolyn Buchwald[d,e], Scott D. Wankel[d], Alyson E. Santoro[e], Julius Sebastian Lipp[b,c], Kai-Uwe Hinrichs[b,c], and Ann Pearson[a,1]

[a]Department of Earth and Planetary Sciences, Harvard University, Cambridge, MA 02138; [b]Organic Geochemistry Group, MARUM–Center for Marine Environmental Sciences, University of Bremen, Bremen 28359, Germany; [c]Department of Geosciences, University of Bremen, Bremen 28359, Germany; [d]Department of Marine Chemistry and Geochemistry, Woods Hole Oceanographic Institution, Woods Hole, MA 02543; and [e]Horn Point Laboratory, University of Maryland Center for Environmental Science, Cambridge, MD 21613

Edited by Katherine H. Freeman, Pennsylvania State University, University Park, PA, and approved May 10, 2016 (received for review September 17, 2015)

Archaeal membrane lipids known as glycerol dibiphytanyl glycerol tetraethers (GDGTs) are the basis of the TEX_{86} paleotemperature proxy. Because GDGTs preserved in marine sediments are thought to originate mainly from planktonic, ammonia-oxidizing Thaumarchaeota, the basis of the correlation between TEX_{86} and sea surface temperature (SST) remains unresolved: How does TEX_{86} predict surface temperatures, when maximum thaumarchaeal activity occurs below the surface mixed layer and TEX_{86} does not covary with in situ growth temperatures? Here we used isothermal studies of the model thaumarchaeon *Nitrosopumilus maritimus* SCM1 to investigate how GDGT composition changes in response to ammonia oxidation rate. We used continuous culture methods to avoid potential confounding variables that can be associated with experiments in batch cultures. The results show that the ring index scales inversely (R^2 = 0.82) with ammonia oxidation rate (ϕ), indicating that GDGT cyclization depends on available reducing power. Correspondingly, the TEX_{86} ratio decreases by an equivalent of 5.4 °C of calculated temperature over a 5.5 fmol·cell^{-1}·d^{-1} increase in ϕ. This finding reconciles other recent experiments that have identified growth stage and oxygen availability as variables affecting TEX_{86}. Depth profiles from the marine water column show minimum TEX_{86} values at the depth of maximum nitrification rates, consistent with our chemostat results. Our findings suggest that the TEX_{86} signal exported from the water column is influenced by the dynamics of ammonia oxidation. Thus, the global TEX_{86}–SST calibration potentially represents a composite of regional correlations based on nutrient dynamics and global correlations based on archaeal community composition and temperature.

Thaumarchaeota | TEX_{86} | GDGT | continuous culture | nitrification

The glycerol dibiphytanyl glycerol tetraether (GDGT) membrane lipids of Archaea are abundant in marine water columns and sediments. The major source of GDGTs to ocean sediments is thought to be planktonic, ammonia-oxidizing Archaea (AOA) affiliated with the phylum Thaumarchaeota (formerly Marine Group I Crenarchaeota) (1, 2). Thaumarchaeota play a primary role in the nitrogen cycle, performing the first and rate-limiting step of nitrification—namely, the oxidation of ammonia to nitrite (3–5). Accordingly, Thaumarchaeota are most abundant at the base of, or below, the euphotic zone (6–9). Based on the phylogeny of their ammonia monooxygenase gene, the planktonic Thaumarchaeota are divided into two distinct clusters, the Water Column Cluster A that is most abundant in the epi- and upper mesopelagic (above ∼200 to ∼500 m, depending on location) and the Water Column Cluster B that dominates thaumarchaeal assemblages in the deeper mesopelagic and bathypelagic (7–10). These clusters putatively represent thaumarchaeal ecotypes adapted to high and low ammonium flux, respectively (11, 12).

Thaumarchaeota produce GDGTs containing from zero to four cyclopentane rings (GDGT-0 to GDGT-4) or four cyclopentane rings and one additional cyclohexane ring (e.g., in crenarchaeol; see *SI Appendix*, Fig. S1). The ratio between a specific subset of these GDGTs is the basis of the TEX_{86} paleothermometer, which assumes that planktonic Archaea adapt to higher growth temperatures by increasing cyclization in their GDGT membrane lipids (see *SI Appendix*, Eq. **S3** (13). This proxy is calibrated to either annual mean sea surface or subsurface temperature using modern surface sediments (e.g., 0–200 m; see *SI Appendix*, Eq. **S4**) (14, 15) and has been used for paleoclimate reconstructions over the past 100 Ma (16). Trends in reconstructed TEX_{86} temperatures often agree well with other proxy records but can diverge, particularly during greenhouse climates (17, 18).

Despite its wide application, the mechanistic basis of the TEX_{86} proxy remains unresolved. Culture studies have shown that the average number of cyclopentyl moieties in GDGTs can increase with growth temperature in marine Archaea (19–22); however, TEX_{86} values of suspended particulate material (SPM) through the water column do not reflect in situ temperatures either in trend or in magnitude (23–29). TEX_{86}-calculated temperatures in sinking particles and core-top sediments are often colder than mean annual average, especially in highly productive regions such as upwelling systems (30–33). TEX_{86}-calculated temperatures also often reach their maximum values below 200 m, and at these depths, TEX_{86} can yield temperatures that are greater than local sea surface temperatures (23, 26, 28, 34). These patterns indicate that variables other than surface or shallow subsurface temperatures are important in determining environmental TEX_{86} signals.

A clue to explaining these observations comes from batch cultures of marine Thaumarchaeota. TEX_{86} values increase in later growth phases (35) and at lower O_2 concentrations (22). The commonality between these experiments is that both experienced a variable rate of energy supply. Because energy limitation has been

Significance

The membrane lipids of marine Archaea form the basis of the temperature proxy called TEX_{86}, which is used for paleoclimate reconstructions from the Jurassic to the present. To date there remains no satisfactory explanation for how planktonic Archaea are able to record water column temperatures, because TEX_{86} does not correlate well with in situ growth temperatures in the modern ocean. Here we show that the TEX_{86} lipid ratio changes in response to cellular growth rate, which is controlled by the ammonia oxidation rate. This implies that variation in the TEX_{86} ratio with water depth is influenced by the metabolic activity of Thaumarchaeota in the water column.

Author contributions: S.J.H., F.J.E., M.K., K.-U.H., and A.P. designed research; S.J.H., F.J.E., C.B., S.D.W., A.E.S., and J.S.L. performed research; S.J.H., F.J.E., and A.P. analyzed data; and S.J.H., F.J.E., M.K., K.-U.H., and A.P. wrote the paper.

The authors declare no conflict of interest.

This article is a PNAS Direct Submission.

[1]To whom correspondence may be addressed. Email: shurley@fas.harvard.edu, felling@uni-bremen.de, or pearson@eps.harvard.edu.

[2]S.J.H. and F.J.E. contributed equally to this work.

This article contains supporting information online at www.pnas.org/lookup/suppl/doi:10.1073/pnas.1518534113/-/DCSupplemental.

suggested to be a defining feature of the domain Archaea (36) and GDGTs effectively reduce proton permeability and hence promote energy conservation (37, 38), we hypothesized that availability of adequate reducing equivalents, generated via an energy-dependent reverse electron flow from ammonia, could have a direct effect on GDGT distributions.

Here we performed a continuous culture (chemostat) experiment to isolate the influence of energy and e^--donor supply on the lipid composition of the marine AOA *Nitrosopumilus maritimus* SCM1. Chemostat approaches have been valuable in characterizing the response of marine taxa to changing CO_2 concentrations (39) and to nutrient limitation (40), each with the objective of isolating a component of physiological response. In our experiments with *N. maritimus*, the chemostat not only controls the growth and corresponding ammonia oxidation rate but also maintains the thermal and chemical stability of the growth conditions. This approach is fundamentally different from all previous batch culture (21, 22, 35) and mesocosm (19, 20) studies of GDGT-producing planktonic Archaea, in which several potentially competing variables such as metabolic activity, temperature, community assemblage, and chemical composition of the medium simultaneously could have influenced the lipid distributions.

Results

Lipid Response to Controlled Energy Supply. We cultivated an isothermal (28 °C) continuous culture of *N. maritimus* (see *SI Appendix*, Fig. S2) to steady state at each of three dilution rates, corresponding to doubling times (T_d) of 71 h (slow growth rate), 30 h (intermediate growth rate), and 22 h (fast growth rate), thereby maintaining the system in continuous culture for 6 mo over the course of the experiments. Nearly identical cell concentrations (1.4–2.0 10^7 cells·mL^{-1}; see *SI Appendix*, Fig. S3 and Table S1) were achieved at the different growth rates by limited provision of ammonia (inflow ca. 150 μM). Cell-specific ammonia oxidation rates, as measured by the production of NO_2^-, were 1.6, 3.9, and 7.1 fmol cell^{-1}·d^{-1}, respectively. The concentration of NO_2^- in the chemostat varied by a maximum of 7% across all stages (mean value, 132.5 μM), and the pH remained within 0.07 units of the mean value (7.64). Biomass harvested during each growth rate was directly hydrolyzed to remove polar head groups and obtain total GDGTs, whereas nonhydrolyzed biomass was extracted to measure respiratory quinones and intact polar GDGTs (for structures, see *SI Appendix*, Fig. S1).

The relative abundance of respiratory menaquinones (MK; see *SI Appendix*, Fig. S1)—isoprenoid lipids that act as intramembrane electron and proton carriers within the thaumarchaeal respiratory chain (41)—decreased at lower ammonia oxidation rates (ϕ), representing between 1.0% and 2.5% of total lipids (Fig. 1*A*). This is consistent with a down-regulated electron transport chain in more slowly metabolizing cells.

The cyclization of total GDGTs, or the relative number of cycloalkyl moieties known as the ring index (RI), decreased at higher ammonia oxidation rates (Fig. 1 *B* and *C*). This reflects an underlying decrease in the cyclization of individual intact polar GDGTs and core GDGTs (see *SI Appendix*, Fig. S4). However, the relative abundance of different intact polar GDGT classes did not change systematically with ammonia oxidation rate (see *SI Appendix*, Fig. S4). Therefore, the cyclization trend in total GDGTs represents the individual response of the most abundant intact polar GDGT classes. The cumulative effect in total GDGTs was a decrease in the most abundant GDGT structures, crenarchaeol and GDGT-2, at the benefit of GDGT-0 and GDGT-1, with increasing ammonia oxidation rates. GDGTs of minor abundance (GDGT-3 and the crenarchaeol regioisomer) did not show a systematic variation with ammonia oxidation rate. Accordingly, the GDGT RI (see *SI Appendix*, Eq. **S5**) decreased with higher ammonia oxidation rates (Fig. 1*B*), and the RI calculated only from GDGTs with zero to four cyclopentane rings (GDGT-0 to GDGT-4; see *SI Appendix*, Eq. **S6**) had a similar response to ϕ (Fig. 1*C*).

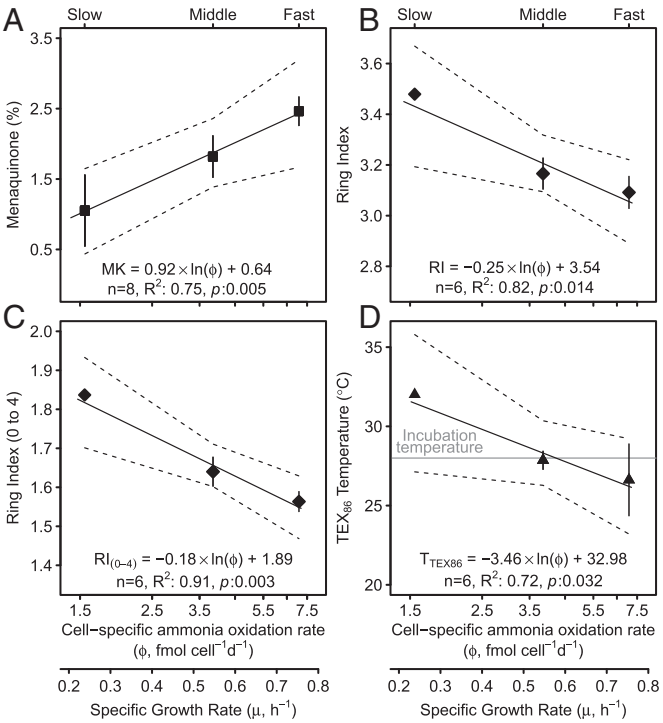

Fig. 1. Ratios of total GDGTs obtained from hydrolyzed lipid extract or biomass vary as a function of cell-specific ammonia oxidation rate (ϕ) and specific growth rate (μ) in an isothermal continuous culture of *N. maritimus*. The abundance of respiratory quinones (MK, relative to total lipids) increases at higher ammonia oxidation rate (*A*). The RI (*B*), RI of GDGT-0 to -4 only (*C*), and TEX_{86}-calculated temperatures (*D*) decrease at higher ammonia oxidation rates. Dashed lines represent 95% confidence intervals on the regression fit through all harvests.

The TEX_{86} ratio is a modified form of the RI incorporating only the GDGTs of minor abundance. Similar to the trend observed in the RI, calculated TEX_{86} temperatures were "colder" at higher ammonia oxidation rates (i.e., faster growth rates) and "warmer" at low ammonia oxidation rates. TEX_{86}-calculated temperatures ranged from 32.0 °C during the slow growth rate to 26.6 °C during the fast growth rate, representing up to 4 °C deviation from the actual growth temperature of 28 °C (Fig. 1*D*). The relationship between TEX_{86}-derived temperature and cell-specific ammonia oxidation rate was logarithmic:

$$T_{TEX86} = -3.46 \cdot \ln(\phi) + 32.98;\ R^2 = 0.72,\ P = 0.032, n = 6. \quad \textbf{[1]}$$

Implications for Previous Batch Culture Experiments. Batch cultures of the same thaumarchaeal strain (*N. maritimus* SCM1) grown at different metabolic energy levels provide the closest experimental analogs to our chemostat results. Elling et al. (35) showed that the apparent temperature calculated from TEX_{86} values increases over the course of a batch culture. Harvesting batch cultures during successive growth phases (i.e., early growth, late growth, and stationary phase) presumably samples decreasing ammonia oxidation rates in a system that is becoming more energy-limited as the ammonia supply is used up (35). We estimated the ammonia oxidation rates for the different growth phases from the reported TEX_{86} temperatures using Eq. **1**. This resulted in estimated cell-specific ammonia oxidation rates that decrease by ca. 12 fmol cell^{-1}·d^{-1} from the early growth phase, when there is excess substrate, to the stationary phase, when the substrate is depleted (Fig. 2*A*). We then used the published cell densities and time-dependent NO_2^- concentrations from ref. 35 to independently calculate the experimental ammonia oxidation

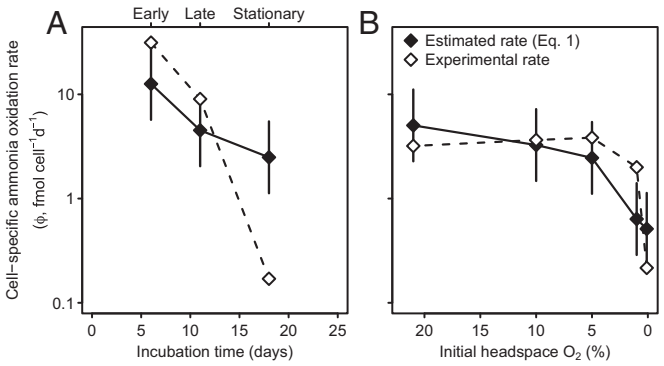

Fig. 2. Ammonia oxidation rates of previously published batch culture experiments (22, 35) estimated from measured TEX_{86} values using the relationship of Eq. **1** (black diamonds) are shown relative to the oxidation rates determined from data reported for these experiments (experimental rate), as calculated from cell densities and the time-dependent concentration of NO_2^- (white diamonds). Batch cultures from ref. 35 yield lower ammonia oxidation rates (higher TEX_{86} values) in later growth phases as the ammonia supply is depleted (*A*). Batch cultures from ref. 22 under oxygen limitation similarly yield lower ammonia oxidation rates (higher TEX_{86} values) as O_2 decreases (*B*). Error bars represent propagated error from Eq. **1** calculated by converting the average width of the confidence interval (Fig. 1) into the cell-specific ammonia oxidation rates.

rates and compare them to the TEX_{86}-derived estimates. The experimental ammonia oxidation rates similarly decreased from early growth phase to stationary phase, however the magnitude of change was somewhat greater than the estimated rates from the TEX_{86} data and Eq. **1**.

Qin et al. (22) showed that the apparent temperature calculated from TEX_{86} values increases in batch cultures incubated with lower headspace O_2 concentrations. Varying the O_2 concentration should similarly control the ammonia oxidation rate by limiting the availability of e^--acceptor, instead of (or colimiting with) the e^--donor. The cell-specific ammonia oxidation rates estimated from the reported TEX_{86} values and Eq. **1** decrease by ca. 5 fmol $cell^{-1}{\cdot}d^{-1}$ under oxygen-limiting conditions (Fig. 2*B*). These estimated rates agree well with the experimental ammonia oxidation rates determined from ref. 22 using the reported cell densities and NO_2^- concentrations.

In all three culture systems—chemostat, high-nutrient batch (35), and O_2-limiting batch (22)—the trends in TEX_{86}-estimated ammonia oxidation rates are consistent with experimental ammonia oxidation rates. These experiments with *N. maritimus* point to a common TEX_{86} response, in which TEX_{86}-derived temperatures decrease as ammonia oxidation rate increases.

Applicability to Marine Water Columns. Cell-specific ammonia oxidation rates in the chemostat (1.6–7.1 fmol $cell^{-1}{\cdot}d^{-1}$), as well as those estimated for previous batch cultures (22, 35), fall well within activities of natural assemblages in pelagic and coastal settings (0.2–15 and 10 fmol $cell^{-1}{\cdot}d^{-1}$, respectively) (8, 10). The slow ammonia oxidation rate additionally resembled the pelagic AOA enrichment, *Candidatus* Nitrosopelagicus brevis (2 fmol NO_2^- $cell^{-1}{\cdot}d^{-1}$; Td, 98 h) (42, 43), as well as North Sea enrichments (2–4 fmol NO_2^- $cell^{-1}{\cdot}d^{-1}$) (44).

To examine the relationship between TEX_{86} ratios and ammonia oxidation rates in the environment, we measured GDGTs, NO_2^- concentrations, in situ temperatures, and nitrification rates for the upper water column of two locations in the South Atlantic Ocean (Fig. 3) (45). We calculated a mass-weighted integration of TEX_{86} values to approximate the export signal from the upper water column (see *SI Appendix*) and compared it to the nearest sedimentary value from the global calibration dataset (46). At station 15, the integrated and sedimentary TEX_{86} values (22.1 °C and 23.8 °C; Fig. 3, black and red triangles, respectively) are colder than measured SST (28.9 °C; Fig. 3, column 4), potentially due to productivity differences associated with equatorial upwelling (see *SI Appendix*, Fig. S5). At station 7, in the oligotrophic gyre, the integrated TEX_{86} temperature and the nearest sedimentary TEX_{86} value (29.8 °C and 26.5 °C, respectively) agree with measured SST within calibration error (27.4 °C; Fig. 3, column 4). GDGT abundances and TEX_{86} profiles from these stations showed depth-dependent features consistent with nitrification rates and NO_2^- concentrations. The abundance of GDGTs was low in surface waters and highest just below the depth of maximum NO_2^- concentrations and maximum measured nitrification rates (Fig. 3, columns 1–3, blue shading). TEX_{86} values decreased between surface waters and the zone of maximum nitrification rates. Minimum TEX_{86}-calculated temperatures were observed coincident with maximum NO_2^- concentrations. Below this depth, TEX_{86}-calculated temperatures increased by ~7–12 °C through at least 250 m, consistent with decreasing nitrification rates. Over the same depth range, however, in situ temperatures decreased by 5 °C. Similar observations of a TEX_{86} minimum and an inflection of the TEX_{86} profile near the NO_2^- concentration maximum have been made in other water columns sampled at high resolution (e.g., refs. 28, 34), suggesting that this is a ubiquitous phenomenon.

Discussion

The RI describes the relative numbers of cycloalkyl rings within the biphytanyl moieties of GDGTs. Because thermophilic Archaea use cyclization as an adaptation to growth temperature (47, 48), the similarly formulated TEX_{86} ratio was assumed to depend primarily on growth temperature in marine Archaea (13). Although it is now acknowledged that other factors such as community dynamics (e.g., refs. 29, 34) may affect TEX_{86} and that in situ temperatures and TEX_{86} are decoupled in the global subsurface ocean (23–28), these arguments remain centered around a temperature-driven response.

The temperature response argument was initially supported by the correlation of TEX_{86} with in situ temperatures in the surface ocean (0–100 m), as this strong correlation (R^2 = 0.75) had a linear slope similar to the global core top calibration (24). However, no such correlation was found for water depths below 100 m, and updating this calibration to include all published SPM data shows that the relationship between 0–100 m is weaker than the early data indicated (see *SI Appendix*, Fig. S6). The cumulative data show that the TEX_{86} ratio of intact polar GDGTs is not correlated to temperature and that the coefficient of determination values for core GDGTs—irrespective of the chosen depth interval (0–100 m or 0–200 m)—are much lower (R^2 = 0.56 or 0.40) than either the initial SPM or core-top calibrations (13–15, 24). Therefore factors other than growth temperature likely exert significant influence on GDGT distributions and the TEX_{86} core-top calibration, especially when considering that the sedimentary record includes additional confounding factors such as production of GDGTs throughout the water column, changes in community composition, and selective export mechanisms (e.g., refs. 18, 25, 29, 34).

Energy limitation has been suggested to be a defining feature of Archaea, and maintaining low proton permeability of their membranes is a common need of both thermophilic Archaea and of mesophilic Thaumarchaeota (36). Remarkably, mesophilic Thaumarchaeota and thermophilic Archaea seem to use the same mechanism, GDGT cyclization, to regulate membrane fluidity and proton permeability (21, 22, 37, 38, 47). At the depth of maximum thaumarchaeal activity, between 50 and 200 m (e.g., 7, 10), most ocean waters have temperatures between 5 and 15 °C (with the exception of polar latitudes). These temperatures are much colder and represent a smaller dynamic range than experiments performed with thermophiles, yet GDGTs of marine Archaea consistently have higher RI values than thermophiles (22, 35, 47). The high RI of marine mesophilic Thaumarchaeota as well as increasing TEX_{86} values in later growth phases (35) and at lower O_2 concentrations (22) suggest that energy conservation may be an important factor influencing GDGT composition in these Archaea.

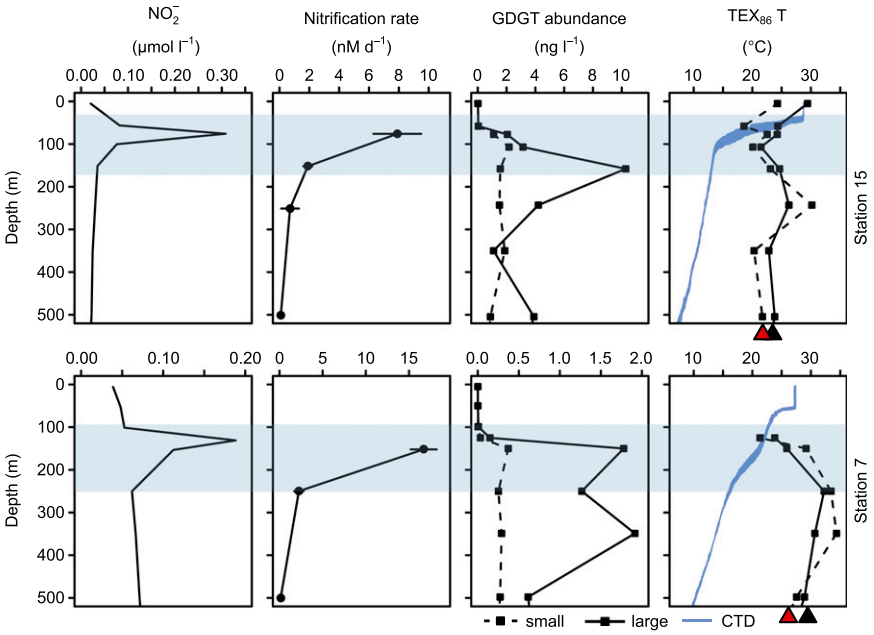

Fig. 3. South Atlantic Ocean water column properties support the relationship between TEX_{86} and ammonia oxidation rate (22.5°S 33.0°W: station 7; 2.7°S 28.5°W: station 15). Column 1: NO_2^- concentrations. Column 2: Measured nitrification rates (refer to *SI Appendix* for methods). Column 3: GDGT abundance in small (0.3–0.7 μm, dotted line) and large (0.7–53 μm, solid line) suspended particulate size classes. Column 4: TEX_{86} values from small and large size classes compared with in situ measured temperatures (blue line). The zone of maximum nitrification rates, NO_2^- concentrations, and TEX_{86} minima is highlighted by the light blue horizontal shading. Red triangles represent the nearest sediment TEX_{86} values compiled from ref. 46, whereas black triangles represent the integrated TEX_{86} value from 0 to 500 m.

Cellular Energy Balance and the Synthesis of GDGTs: The Reducing Power-Limitation Hypothesis. The in situ energetic stress imposed by low ammonia and/or O_2 availability, as well as the intrinsically low energetic yield of ammonia oxidation, may qualify the Thaumarchaeota as energetic extremophiles (36). This idea is consistent with studies that show a low half-saturation constant (K_m; NH_3 + NH_4^+) of 98–132 nM for ammonia oxidation by *N. maritimus* (49, 50), and it suggests adaptation to growth under conditions of constantly low energy flux, as typically found in open ocean waters. *N. maritimus* (as well as all recently characterized Thaumarchaeota) fixes inorganic carbon using an energy-efficient hydroxypropionate/hydroxybutyrate (HP/HB) pathway that minimizes input of chemical energy from ATP and yields the products acetate (HP/HB full cycle) and succinate (HP half cycle) (43, 51). The results of our chemostat experiments are consistent with this view of broad metabolic adaptation to energy stress in Thaumarchaeota. How, then, does this observation explain GDGT lipid ratios, in which RI and TEX_{86} values increase at greater ammonia limitation? In addition to promoting energy conservation through decreased proton permeability, we argue that there may also be a biosynthetic explanation.

Most chemolithotrophs conserve only a small fraction of the energy obtained from the respiration of inorganic substrates—that is, most of the energy flux is dissimilatory. From the conserved fraction, they must generate reducing power for biosynthetic processes, and in most cases, including AOA, this requires energy-dependent reverse electron transport. For example, the electrochemical potential of the NH_4^+/NO_2^- redox couple is insufficient to reduce $NAD(P)^+$ to $NAD(P)H_2$. However, the synthesis of GDGT-0 from two molecules of the intermediate digeranylgeranyl glycerol-1-phosphate (DGGGP) requires 14 H_2 equivalents in a reduction reaction mediated by the enzyme geranylgeranyl reductase (GGR; Fig. 4) (52, 53). The cofactor for GGR is $FADH_2$, and it is most likely regenerated by e^- supplied by $NAD(P)H_2$ (54). Thus, the saturation step in GDGT synthesis requires the cell to supply not only e^- but also additional chemical energy (ATP) and/or proton-motive force to rereduce the cofactors; the energetic needs may be similar to transhydrogenation in bacteria (55).

Lipid biosynthesis is only one of many components of cellular metabolism in ammonia-oxidizing Thaumarchaeota that require ATP- or proton motive force-dependent reverse electron flow. All of these pathways are in direct competition for both e^- and energy—the scarcity of which has been proposed as motivation for the evolution of the HP/HB pathway (51). The presence of cyclopentane rings in GDGTs may be viewed as a strategy to reduce demand for e^- and energy as well as in the more traditional sense of maintaining low proton permeability (37, 48). In this way, adaptation to e^--donor limitation in Thaumarchaeota and to higher growth temperatures in both Thaumarchaeota and archaeal thermophiles operates via the same mechanism: It reduces proton permeability by increasing the packing density of membrane lipids (38). If there is an insufficient rate of $FADH_2$ regeneration under energy-limited conditions, DGGGP may form a cycloalkyl ring rather than saturating the double bond, thereby saving 2 e^- (Fig. 4*B*).

Although speculative, this hypothesis offers a direct, mechanistic explanation for greater numbers of cycloalkyl rings at lower ammonia oxidation rates. The idea may be testable through measurements of natural hydrogen isotope fractionation as an indicator of cellular hydrogenase activity (56). Our chemostat data, as well as previous batch culture studies from which oxidation rates may be inferred (Fig. 2) (22, 35) also point to the plausibility of this hypothesis, as the RI scales directly with respiratory activity as expressed in the abundance of the electron carrier MK (Fig. 1*A*). Further, RIs calculated with and without crenarchaeol yield the same slopes, suggesting that the cyclohexyl-bearing crenarchaeol may serve a similar physiological role as cyclopentyl-containing GDGTs (Fig. 1 *B* and *C*).

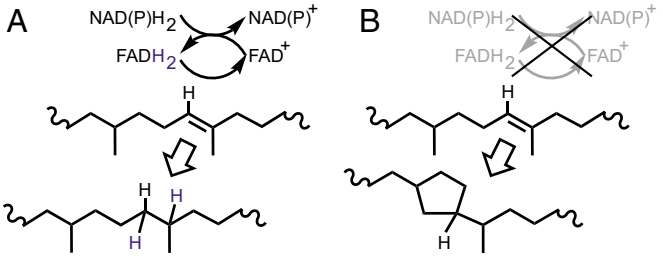

Fig. 4. Proposed synthesis of GDGT-0 from two molecules of DGGGP includes a saturation step (*A*) mediated by GGR and requiring the cofactors $FADH_2$ and $NAD(P)H_2$. Electron limitation (*B*) may slow the regeneration of one or more of these cofactors, causing internal cyclization rather than saturation.

Environmental Implications. The relationship between GDGT cyclization and energy limitation observed in *N. maritimus* provides a long sought-after mechanism to explain the directionality of water column TEX_{86} patterns. Water column profiles typically show inflections in apparent TEX_{86} temperatures, first falling toward the NO_2^- maximum, while temperature is also decreasing, and then rising below this point, while temperature continues to decrease (Fig. 3) (23, 28, 34). Invoking a temperature-only control is not sufficient to explain patterns of water column TEX_{86}. In contrast, ammonia oxidation rate can uniquely explain the directionality of the observed TEX_{86} changes with depth. Although it is possible that the ammonia oxidation rate itself depends on temperature—essentially rendering oxidation and temperature inseparable variables—the kinetic response of ammonia oxidation rate to increasing temperature appears to be insignificant in natural marine communities (50). The TEX_{86}–temperature relationship inferred from core-top sediments may represent the interplay of several variables (e.g., ammonia oxidation rate, temperature, export depth) or the covariation of temperature and TEX_{86} with other, latitude-dependent, oceanographic and ecological parameters.

Our results suggest that the process of GDGT cyclization in the marine water column is not directly controlled by growth temperature, while simultaneously explaining how an apparent link to temperature may arise. Net primary production varies in response to density stratification and its effect on nutrient exchange through vertical mixing (57). This explains why warm environments with lower rates of primary production and subphotic zone nutrient regeneration—that is, lower ammonia oxidation rates (8, 58)—have warm TEX_{86}-calibrated SSTs. Similarly, TEX_{86} warming observed within oxygen minimum zones is likely caused by energy stress and a corresponding decrease in ammonia oxidation rates; that is, it is not directly caused by physiological response to low O_2 as suggested by Qin et al. (22). This explains why the subsurface TEX_{86} warming trend also is observed in well-oxygenated water columns and not limited only to oxygen minimum zones (23, 27). In contrast, cold TEX_{86} temperatures are observed in surface sediments and SPM at high-nutrient/high-productivity sites such as upwelling systems (e.g., refs. 30–33).

Further experiments with a broader range of thaumarchaeal ecotypes are necessary to understand the global relationship between TEX_{86}, ammonia oxidation rates, and temperature. *N. maritimus* was isolated from a tropical fish tank in the Seattle aquarium (3) and displays a narrow growth range (~20–30 °C) and a high temperature optimum (28 °C), which is particularly applicable to the low latitude environment studied here. However, the global TEX_{86} calibration encompasses temperate and polar eco- and phylotypes (e.g., ref. 59) that may exhibit different magnitudes for the relationship between TEX_{86} and ammonia oxidation rate (Eq. **1**), as evidenced by latitude-dependent and ocean basin-dependent TEX_{86} patterns (15, 18). Further, the range of ammonia oxidation rates observed in the ocean (8, 10) is much larger than in our culture system, indicating that the range of TEX_{86} changes that might be attributable to metabolic activity is likely larger than shown here for *N. maritimus*.

Indeed, previous studies indicate that GDGT composition may significantly vary even between different strains of cultured planktonic Thaumarchaeota (21, 22). The transition from shallow-water to deep-water thaumarchaeal ecotypes has been invoked to explain different relative GDGT compositions through the water column (e.g., refs. 29, 34). However, the major shift to the deep thaumarchaeal eco- and phylotype occurs well below the typical abundance and activity maxima and below the depth where TEX_{86} is typically most variable (e.g., refs. 6–9, 11, 12). The fact that the inverse correlation between TEX_{86} and ammonia oxidation rate determined for a single taxon, *N. maritimus*, agrees with the overall patterns of TEX_{86} values produced by natural assemblages in the marine water column suggests that it may represent a universal mechanism. Thus, the TEX_{86} inflection in the zone of maximum nitrification is likely not influenced, or only secondarily influenced, by variations in community composition.

The latitudinal distribution of thaumarchaeal ecotypes suggests that there are regionally distinct populations: Low-ammonia adapted ecotypes predominate in less productive, stratified regions such as subtropical gyres and deep water (ca. >200–500 m), whereas high-ammonia adapted ecotypes dominate more productive sites such as subpolar and equatorial upwelling regions (11, 12). Differences in the TEX_{86}–ammonia oxidation rate responses of these ecotypes potentially offer an explanation for regional TEX_{86}–temperature correlations. In addition to focusing on depth distributions of ecotypes, future work also will need to focus on the influence these spatial trends in thaumarchaeal ecology have on GDGT distributions.

Currently, regional or spatially variable calibration models appear to be the most reasonable choice for paleotemperature reconstructions, as they account for modern variations in hydrographic and ecological effects. It may be challenging to accurately interpret TEX_{86} records in past ocean regimes in which circulation-driven nutrient regeneration rates or total global nutrient budgets may have defined spatially and temporally distinct TEX_{86} correlations. Thus, the development of calibration models based on analogous biogeochemical environments is highly warranted for assessing the complex ecological effects amalgamated into the TEX_{86} ratio and for improving our ability to reconstruct past climate.

Materials and Methods

N. maritimus SCM1 was maintained at 28 °C and pH 7.6 in the dark in a 4.5-l chemostat containing Synthetic Crenarchaeota Medium (150 μM NH_4^+; see *SI Appendix, SI Materials and Methods* and Fig. S2). Specific growth rate (d^{-1}) was controlled by dilution with fresh medium, and three steady-state experiments were performed (slow growth rate, 0.23 d^{-1}, 71 h T_d; intermediate growth rate, 0.56 d^{-1}, 30 h T_d; fast growth rate, 0.75 d^{-1}, 22 h T_d) (*SI Appendix*, Fig. S3).

Depth profiles of (SPM) samples were retrieved from a latitudinal transect through the Atlantic Ocean (see *SI Appendix*, Fig. S5) using in situ pumps equipped with a sequence of filters (53 μm, 0.7 μm, 0.3 μm). Lipids were extracted from biomass harvested from chemostat effluent by cross-flow filtration or centrifugation. Intact polar lipids and quinones from biomass and SPM were analyzed using reversed-phase HPLC–MS. Core lipids extracted from hydrolyzed biomass were analyzed using normal-phase HPLC–MS. For details, see *SI Appendix*.

ACKNOWLEDGMENTS. The authors thank the editor and three anonymous reviewers for providing comments that helped improve earlier versions of this manuscript. The authors thank Joe Jennings (Oregon State University) for nitrite concentrations. Funding for the cruise was provided by the National Science Foundation (Grant OCE-1154320; to E. Kujawinski and K. Longnecker, WHOI). This research was supported by the Deutsche Forschungsgemeinschaft through the Gottfried Wilhelm Leibniz Program (Award to K.-U.H.; Hi 616-14-1, funds for F.J.E., M.K., construction of chemostat, and acquisition of ABSciEX QTRAP4500 mass spectrometer) and Instrument Grant Inst 144/300-1 (quadrupole TOF–MS). A.P. and S.J.H. acknowledge funding from the National Science Foundation (Grant OCE-1129343), the Gordon and Betty Moore Foundation, an EAOG travel fellowship, and the NASA Astrobiology Institute. A.E.S. and C.B. acknowledge funding from the National Science Foundation (Grant OCE-1260006).

1. Brochier-Armanet C, Boussau B, Gribaldo S, Forterre P (2008) Mesophilic Crenarchaeota: Proposal for a third archaeal phylum, the Thaumarchaeota. *Nat Rev Microbiol* 6(3):245–252.
2. Spang A, et al. (2010) Distinct gene set in two different lineages of ammonia-oxidizing archaea supports the phylum Thaumarchaeota. *Trends Microbiol* 18(8):331–340.
3. Könneke M, et al. (2005) Isolation of an autotrophic ammonia-oxidizing marine archaeon. *Nature* 437(7058):543–546.
4. Beman JM, Popp BN, Francis CA (2008) Molecular and biogeochemical evidence for ammonia oxidation by marine Crenarchaeota in the Gulf of California. *ISME J* 2(4):429–441.
5. Newell SE, Fawcett SE, Ward BB (2013) Depth distribution of ammonia oxidation rates and ammonia-oxidizer community composition in the Sargasso Sea. *Limnol Oceanogr* 58(4):1491–1500.
6. Church MJ, Wai B, Karl DM, DeLong EF (2010) Abundances of crenarchaeal *amoA* genes and transcripts in the Pacific Ocean. *Environ Microbiol* 12(3):679–688.
7. Francis CA, Roberts KJ, Beman JM, Santoro AE, Oakley BB (2005) Ubiquity and diversity of ammonia-oxidizing archaea in water columns and sediments of the ocean. *Proc Natl Acad Sci USA* 102(41):14683–14688.

8. Santoro AE, Casciotti KL, Francis CA (2010) Activity, abundance and diversity of nitrifying archaea and bacteria in the central California Current. *Environ Microbiol* 12(7):1989–2006.
9. Smith JM, Damashek J, Chavez FP, Francis CA (2015) Factors influencing nitrification rates and the abundance and transcriptional activity of ammonia-oxidizing microorganisms in the dark northeast Pacific Ocean. *Limnol Oceanogr* 61(2):596–609.
10. Smith JM, Casciotti KL, Chavez FP, Francis CA (2014) Differential contributions of archaeal ammonia oxidizer ecotypes to nitrification in coastal surface waters. *ISME J* 8(8):1704–1714.
11. Sintes E, Bergauer K, De Corte D, Yokokawa T, Herndl GJ (2013) Archaeal *amoA* gene diversity points to distinct biogeography of ammonia-oxidizing Crenarchaeota in the ocean. *Environ Microbiol* 15(5):1647–1658.
12. Sintes E, De Corte D, Haberleitner E, Herndl GJ (2016) Geographic distribution of archaeal ammonia oxidizing ecotypes in the Atlantic Ocean. *Front Microbiol* 7:77.
13. Schouten S, Hopmans EC, Schefuß E, Sinninghe Damsté JS (2002) Distributional variations in marine crenarchaeotal membrane lipids: A new tool for reconstructing ancient sea water temperatures? *Earth Planet Sci Lett* 204(1-2):265–274.
14. Kim J-H, et al. (2010) New indices and calibrations derived from the distribution of crenarchaeal isoprenoid tetraether lipids: Implications for past sea surface temperature reconstructions. *Geochim Cosmochim Acta* 74(16):4639–4654.
15. Tierney JE, Tingley MP (2014) A Bayesian, spatially-varying calibration model for the TEX_{86} proxy. *Geochim Cosmochim Acta* 127:83–106.
16. Jenkyns HC, Schouten-Huibers L, Schouten S, Sinninghe Damsté JS (2012) Warm Middle Jurassic–Early Cretaceous high-latitude sea-surface temperatures from the Southern Ocean. *Clim Past* 8(1):215–226.
17. Schouten S, Hopmans EC, Sinninghe Damsté JS (2013) The organic geochemistry of glycerol dialkyl glycerol tetraether lipids: A review. *Org Geochem* 54:19–61.
18. Pearson A, Ingalls AE (2013) Assessing the use of archaeal lipids as marine environmental proxies. *Annu Rev Earth Planet Sci* 41(1):359–384.
19. Wuchter C, Schouten S, Coolen MJL, Sinninghe Damsté JS (2004) Temperature-dependent variation in the distribution of tetraether membrane lipids of marine Crenarchaeota: Implications for TEX_{86} paleothermometry. *Paleoceanography* 19(4):PA4028.
20. Schouten S, Forster A, Panoto FE, Sinninghe Damsté JS (2007) Towards calibration of the TEX_{86} palaeothermometer for tropical sea surface temperatures in ancient greenhouse worlds. *Org Geochem* 38(9):1537–1546.
21. Elling FJ, Könneke M, Mußmann M, Greve A, Hinrichs K-U (2015) Influence of temperature, pH, and salinity on membrane lipid composition and TEX_{86} of marine planktonic thaumarchaeal isolates. *Geochim Cosmochim Acta* 171:238–255.
22. Qin W, et al. (2015) Confounding effects of oxygen and temperature on the TEX_{86} signature of marine Thaumarchaeota. *Proc Natl Acad Sci USA* 112(35):10979–10984.
23. Basse A, et al. (2014) Distribution of intact and core tetraether lipids in water column profiles of suspended particulate matter off Cape Blanc, NW Africa. *Org Geochem* 72:1–13.
24. Wuchter C, Schouten S, Wakeham SG, Sinninghe Damsté JS (2005) Temporal and spatial variation in tetraether membrane lipids of marine Crenarchaeota in particulate organic matter: Implications for TEX_{86} paleothermometry. *Paleoceanography* 20(3):PA3013.
25. Turich C, et al. (2007) Lipids of marine Archaea: Patterns and provenance in the watercolumn and sediments. *Geochim Cosmochim Acta* 71(13):3272–3291.
26. Schouten S, et al. (2012) Intact polar and core glycerol dibiphytanyl glycerol tetraether lipids in the Arabian Sea oxygen minimum zone: I. Selective preservation and degradation in the water column and consequences for the TEX_{86}. *Geochim Cosmochim Acta* 98:228–243.
27. Hernández-Sánchez MT, et al. (2014) Variations in GDGT distributions through the water column in the South East Atlantic Ocean. *Geochim Cosmochim Acta* 132: 337–348.
28. Xie S, Liu X-L, Schubotz F, Wakeham SG, Hinrichs K-U (2014) Distribution of glycerol ether lipids in the oxygen minimum zone of the Eastern Tropical North Pacific Ocean. *Org Geochem* 71:60–71.
29. Zhu C, et al. (April 28, 2016) Stratification of archaeal membrane lipids in the ocean and implications for adaptation and chemotaxonomy of planktonic archaea. *Environ Microbiol*, 10.1111/1462-2920.13289.
30. Lee KE, et al. (2008) A study of the alkenone, TEX_{86}, and planktonic foraminifera in the Benguela Upwelling System: Implications for past sea surface temperature estimates. *Geochemistry, Geophys Geosystems* 9(10):Q10019.
31. Huguet C, et al. (2007) A study of the TEX_{86} paleothermometer in the water column and sediments of the Santa Barbara Basin, California. *Paleoceanography* 22(3): PA3203.
32. Lopes dos Santos RA, et al. (2010) Glacial–interglacial variability in Atlantic meridional overturning circulation and thermocline adjustments in the tropical North Atlantic. *Earth Planet Sci Lett* 300(3-4):407–414.
33. Leider A, Hinrichs K-U, Mollenhauer G, Versteegh GJM (2010) Core-top calibration of the lipid-based $U^{K'}_{37}$ and TEX_{86} temperature proxies on the southern Italian shelf (SW Adriatic Sea, Gulf of Taranto). *Earth Planet Sci Lett* 300(1-2):112–124.
34. Kim J-H, Villanueva L, Zell C, Sinninghe Damsté JS (2016) Biological source and provenance of deep-water derived isoprenoid tetraether lipids along the Portuguese continental margin. *Geochim Cosmochim Acta* 172:177–204.
35. Elling FJ, et al. (2014) Effects of growth phase on the membrane lipid composition of the thaumarchaeon *Nitrosopumilus maritimus* and their implications for archaeal lipid distributions in the marine environment. *Geochim Cosmochim Acta* 141: 579–597.
36. Valentine DL (2007) Adaptations to energy stress dictate the ecology and evolution of the Archaea. *Nat Rev Microbiol* 5(4):316–323.
37. Elferink MGL, de Wit JG, Driessen AJM, Konings WN (1994) Stability and proton-permeability of liposomes composed of archaeal tetraether lipids. *Biochim Biophys Acta - Biomembr* 1193(2):247–254.
38. Konings WN, Albers SV, Koning S, Driessen AJ (2002) The cell membrane plays a crucial role in survival of bacteria and archaea in extreme environments. *Antonie van Leeuwenhoek* 81(1-4):61–72.
39. Laws EA, Popp BN, Bidigare RR, Kennicutt MC, Macko SA (1995) Dependence of phytoplankton carbon isotopic composition on growth rate and $[CO_2]_{aq}$: Theoretical considerations and experimental results. *Geochim Cosmochim Acta* 59(6):1131–1138.
40. Riegman R, Stolte W, Noordeloos AAM, Slezak D (2000) Nutrient uptake and alkaline phosphatase (EC 3:1:3:1) activity of *Emiliania huxleyi* (Prymnesiophyceae) during growth under N and P limitation in continuous cultures. *J Phycol* 36(1):87–96.
41. Elling FJ, et al. (2016) Respiratory quinones in Archaea: Phylogenetic distribution and application as biomarkers in the marine environment. *Environ Microbiol* 18(2): 692–707.
42. Santoro AE, Casciotti KL (2011) Enrichment and characterization of ammonia-oxidizing archaea from the open ocean: Phylogeny, physiology and stable isotope fractionation. *ISME J* 5(11):1796–1808.
43. Santoro AE, et al. (2015) Genomic and proteomic characterization of "Candidatus Nitrosopelagicus brevis": An ammonia-oxidizing archaeon from the open ocean. *Proc Natl Acad Sci USA* 112(4):1173–1178.
44. Wuchter C, et al. (2006) Archaeal nitrification in the ocean. *Proc Natl Acad Sci USA* 103(33):12317–12322.
45. Kujawinski E, Longnecker K (2013) Dissolved organic matter composition in the deep Atlantic Ocean CTD. Biological and Chemical Oceanography Data System (BCO DMO, WHOI), iPub: December14, 2013. Accessed August 25, 2014 and February 2006 from www.bco-dmo.org/dataset/481164/data.
46. Tierney JE, Tingley MP (2015) A TEX_{86} surface sediment database and extended Bayesian calibration. *Sci Data* 2:150029.
47. Oger PM, Cario A (2013) Adaptation of the membrane in Archaea. *Biophys Chem* 183: 42–56.
48. Chong PL-G (2010) Archaebacterial bipolar tetraether lipids: Physico-chemical and membrane properties. *Chem Phys Lipids* 163(3):253–265.
49. Martens-Habbena W, Berube PM, Urakawa H, de la Torre JR, Stahl DA (2009) Ammonia oxidation kinetics determine niche separation of nitrifying Archaea and Bacteria. *Nature* 461(7266):976–979.
50. Horak REA, et al. (2013) Ammonia oxidation kinetics and temperature sensitivity of a natural marine community dominated by Archaea. *ISME J* 7(10):2023–2033.
51. Könneke M, et al. (2014) Ammonia-oxidizing archaea use the most energy-efficient aerobic pathway for CO_2 fixation. *Proc Natl Acad Sci USA* 111(22):8239–8244.
52. Nishimura Y, Eguchi T (2006) Biosynthesis of archaeal membrane lipids: Digeranylgeranylglycerophospholipid reductase of the thermoacidophilic archaeon *Thermoplasma acidophilum*. *J Biochem* 139(6):1073–1081.
53. Walker CB, et al. (2010) *Nitrosopumilus maritimus* genome reveals unique mechanisms for nitrification and autotrophy in globally distributed marine crenarchaea. *Proc Natl Acad Sci USA* 107(19):8818–8823.
54. Sasaki D, et al. (2011) Structure and mutation analysis of archaeal geranylgeranyl reductase. *J Mol Biol* 409(4):543–557.
55. Wang S, Huang H, Moll J, Thauer RK (2010) $NADP^+$ reduction with reduced ferredoxin and $NADP^+$ reduction with NADH are coupled via an electron-bifurcating enzyme complex in *Clostridium kluyveri*. *J Bacteriol* 192(19):5115–5123.
56. Zhang Z, Sachs JP, Marchetti A (2009) Hydrogen isotope fractionation in freshwater and marine algae: II. Temperature and nitrogen limited growth rate effects. *Org Geochem* 40(3):428–439.
57. Behrenfeld MJ, et al. (2006) Climate-driven trends in contemporary ocean productivity. *Nature* 444(7120):752–755.
58. Newell SE, Babbin AR, Jayakumar A, Ward BB (2011) Ammonia oxidation rates and nitrification in the Arabian Sea. *Global Biogeochem Cycles* 25(4):GB4016.
59. Luo H, et al. (2014) Single-cell genomics shedding light on marine Thaumarchaeota diversification. *ISME J* 8(3):732–736.